Circular Polarization and Nonreciprocal Propagation in Magnetic Media

Gerald F. Dionne, Gary A. Allen, Pamela R. Haddad, Caroline A. Ross, and Benjamin Lax

The polarization of electromagnetic signals is an important feature in the design of modern radar and telecommunications. Standard electromagnetic theory readily shows that a linearly polarized plane wave propagating in free space consists of two equal but counter-rotating components of circular polarization. In magnetized media, these circular modes can be arranged to produce the nonreciprocal propagation effects that are the basic properties of isolator and circulator devices. Independent phase control of right-hand (+) and left-hand (–) circular waves is accomplished by splitting their propagation velocities through differences in the $\varepsilon_{\pm}\mu_{\pm}$ parameter. A phenomenological analysis of the permeability μ and permittivity ε in dispersive media serves to introduce the corresponding magnetic- and electric-dipole mechanisms of interaction length with the propagating signal. As an example of permeability dispersion, a Lincoln Laboratory quasi-optical Faraday-rotation isolator circulator at 35 GHz ($\lambda \sim$ 1 cm) with a garnet-ferrite rotator element is described. At infrared wavelengths (λ = 1.55 μm), where fiber-optic laser sources also require protection by passive isolation of the Faraday-rotation principle, ε rather than μ provides the dispersion, and the frequency is limited to the quantum energies of the electric-dipole atomic transitions peculiar to the molecular structure of the magnetic garnet. For optimum performance, bismuth additions to the garnet chemical formula are usually necessary. Spectroscopic and molecular theory models developed at Lincoln Laboratory to explain the bismuth effects are reviewed. In a concluding section, proposed advances in present technology are discussed in the context of future radar and telecommunications challenges.

The polarization of an electromagnetic wave is an important aspect of its propagation characteristics. In applications that involve radiated beams, such as radar, polarization concerns are critical in the design of the antennas for optimum performance. Factors that influence the choice of polarization include the nature of the target and the features of the propagation environment, such as irregular ground terrain or open water that can corrupt the signal by introducing unwanted reflections. Linear polarization emerges as a natural result of the radiation from an oscillating dipole and is transmitted with its plane of polarization either vertical or horizontal, depending on the specific application. Linear polarization is also readily transmitted through flexible coaxial cable or rigid waveguides in radio frequency (RF) and microwave systems. In recent years the frequency range of electromagnetic communication technology has been extended to the infrared (IR) region in the form of polarized signals emitted by semiconductor lasers and transmitted through optical-fiber networks.

Less familiar uses of polarization occur in the function of passive isolators that protect signal sources or other components from potentially harmful reflec-

tions, and circulator versions that can direct the return signals into the appropriate receiver channels. For RF applications, the magnetic vectors of the two counter-rotating circular-polarization modes of the linear wave, and the way they are affected by the dispersive permeability of a magnetized medium (usually a ferrite), are the keys to the operation of these devices. When the waves are propagating in the direction of magnetization, the individual phase velocities of the counter-rotating modes are split from the unmagnetized value in a positive and negative sense. As a consequence, the differing velocities cause the plane of polarization of the resultant linear wave to undergo a progressive Faraday-rotation effect that is nonreciprocal.

Nonreciprocal propagation effects of magnetic materials also provide isolation functionality in photonic systems. Analogously to the RF circuit applications, isolator devices are necessary in optical communication systems to protect the laser sources from power instabilities. Although the wavelength band is in the near-IR region where the interaction of the electric vector with the dispersive permittivity determines the propagation properties, the phenomenological theory of Faraday rotation for both RF and optical cases is almost identical. To understand the operation of these devices in terms of plane-wave propagation, we begin with a review of polarization fundamentals, followed by an explanation of birefringence in magnetized media, and continue with the development of key relations between Faraday rotation and the medium's permeability and permittivity. We conclude with descriptions of device applications that continue to be of interest to Lincoln Laboratory and the broader scientific community.

Polarization

An electromagnetic wave consists of time-varying electric and magnetic fields that jointly satisfy Maxwell's equations [1]. The electric and magnetic fields are vector quantities that are functions of time and spatial position. In electromagnetic analyses, a harmonic time variation is usually assumed so that the field $\boldsymbol{\mathcal{E}}$ (or $\boldsymbol{\mathcal{H}}$) can be represented via a phasor quantity according to

$$\boldsymbol{\mathcal{E}}(x,y,z,t) = \text{Real}\left\{\mathbf{E}(x,y,z)e^{i\omega t}\right\}, \qquad (1)$$

where ω is the angular frequency and $\boldsymbol{\mathcal{E}}$ denotes the instantaneous electric-field vector, while $\mathbf{E}$ corresponds to its phasor form. Any time variation of an electromagnetic wave can be expressed as a superposition of harmonic solutions according to Fourier theory.

Polarization is an inherent property of an electromagnetic wave that describes the orientation of its electric-field vector as the wave propagates in time. The simplest polarization case is that of linear polarization in which the electric-field vector traces out a line over time. An example of this polarization is a transverse electromagnetic (TEM) plane wave propagating along z in free space with phasor electric- and magnetic-field components along the $\hat{x}$ and $\hat{y}$ unit vector axes given by

$$\mathbf{E}(z) = \hat{x}E_0 e^{-i\beta_0 z} \qquad (2)$$

and

$$\mathbf{H}(z) = \hat{y}H_0 e^{-i\beta_0 z}. \qquad (3)$$

E_0 and H_0 are the amplitudes in free space, and the propagation constant β_0 is the ratio of angular frequency to the velocity of light (ω/c). The phasor form of the electric field given by Equation 2 shows the electromagnetic wave to be linearly polarized along $\hat{x}$. The instantaneous TEM traveling waves derived from Equations 1 through 3 are

$$\boldsymbol{\mathcal{E}}(z,t) = \hat{x}E_0 \cos\left(\omega t - \beta_0 z\right)$$

and

$$\boldsymbol{\mathcal{H}}(z,t) = \hat{y}H_0 \cos\left(\omega t - \beta_0 z\right).$$

A snapshot of the TEM field at time $t = 0$ is illustrated by the orthogonal sinusoidal functions of z in Figure 1, in which the electric-field vector is aligned in the x direction. As time advances, this snapshot effectively moves forward in the z direction corresponding to wave propagation.

Linear polarization is commonly referred to as horizontal or vertical, which describes its orientation within a given reference frame such as relative to a flat earth surface or within a local target coordinate system. Linear polarization oriented horizontally with respect to the earth is often used for upward-looking radar systems performing air surveillance, since this polarization is well matched to the horizontal metal

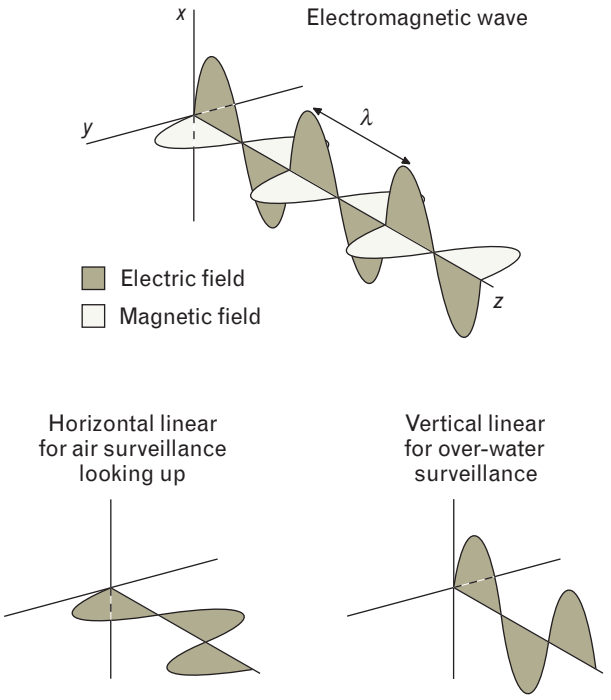

FIGURE 1. Instantaneous ($t = 0$) sinusoidal trace of an electromagnetic signal of wavelength λ directed along the z-axis. The orthogonal electric- and magnetic-field components are shown oscillating along the respective x- and y-axes. The lower two figures show the appropriate electric-field linear polarization for two specific measurement conditions.

structure of an airplane. Vertical polarization in an earth-reference frame is used for over-water surveillance, since it suffers less multipath loss than horizontal polarization. The polarization for a radar application needs to be matched to both the target and the propagation environment.

The orientation of the electric-field vector can change with time as the wave propagates. Two simple TEM plane waves consisting of both x and y electric-field components can be combined to yield a vector that rotates in the x-y plane as the wave propagates forward with time. In the most general case, this electric-field vector traces out an ellipse. However, if the amplitudes and phases of the x and y components satisfy certain conditions, then the electric-field vector can be made to trace out a circle, thereby producing circular polarization. Circular polarization is used in radar applications for polarization diversity and target discrimination, and is used in communications systems to mitigate rain attenuation.

There are two senses of circular polarization, right-hand circular polarization (RHCP) and left-hand circular polarization (LHCP). In Figure 2, these modes are revealed as counter-rotating spirals that sum to form a linearly polarized wave. The handedness property describes the rotation of the electric-field vector (clockwise or counterclockwise) relative to the direction of propagation. If the fingers in a person's right hand curl in the same direction as the rotation of the electric-field vector while the thumb is pointing in the propagation direction, then the wave is right-hand circularly polarized. Similarly, a circularly polarized wave is left handed if the fingers on a person's left hand curl in the direction of electric vector rotation while the thumb points in the direction of propagation.

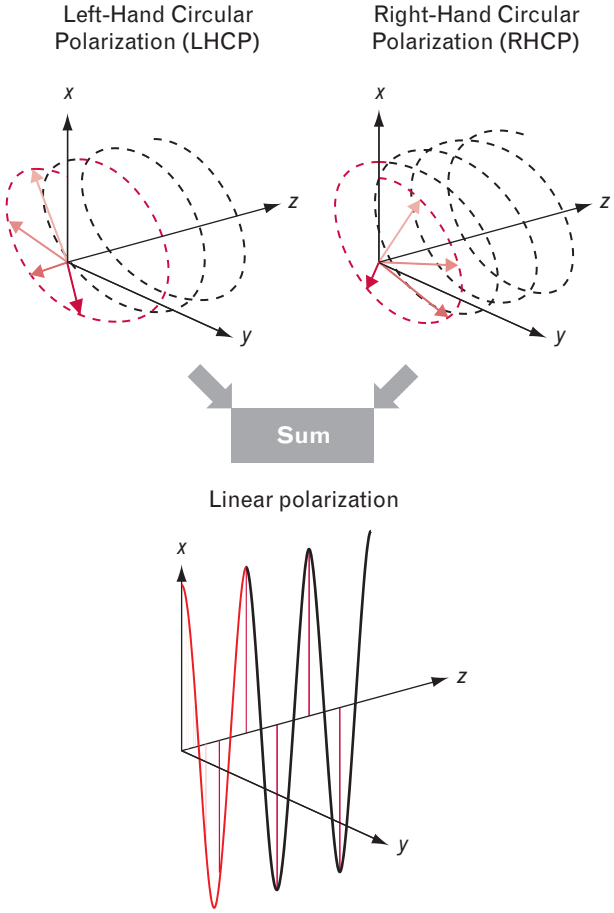

FIGURE 2. Anatomy of the linearly polarized wave shown propagating along the z-axis. The electric-field vectors of two equal-amplitude counter-rotating circularly polarized waves sum to form a parent linear wave of twice the amplitude.

Mathematically, the electric-field phasors for RHCP (+) and LHCP (–) plane waves propagating along z are described respectively by

$$\mathbf{E}_{+}(z) = \frac{1}{2} E_0 \left(\hat{x} - i\hat{y}\right) e^{-i\beta_0 z} \tag{4}$$

and

$$\mathbf{E}_{-}(z) = \frac{1}{2} E_0 \left(\hat{x} + i\hat{y}\right) e^{-i\beta_0 z} \,. \tag{5}$$

Equations 4 and 5 show that circular polarization is achieved when the x and y components of the electric field assume equal amplitudes and are separated in phase by 90°. It is instructive to examine the instantaneous form of these waves. The time-varying electric fields for RHCP and LHCP are given by

$$\boldsymbol{\mathcal{E}}_{\pm}(z,t) = \frac{1}{2} E_0 \left\{ \hat{x} \cos\left(\omega t - \beta_0 z\right) \pm \hat{y} \sin\left(\omega t - \beta_0 z\right) \right\}. \tag{6}$$

In the z = 0 plane, Equation 6 reduces to

$$\boldsymbol{\mathcal{E}}_{\pm}(0,t) = \frac{1}{2} E_0 \left\{ \hat{x} \cos\left(\omega t\right) \pm \hat{y} \sin\left(\omega t\right) \right\}, \tag{7}$$

which describes a circle in the x-y plane that is traced out clockwise (RHCP) or counterclockwise (LHCP) versus time, when the plane is viewed from the negative z direction.

To understand device operations based on the magnetic control of individual circular-polarization phases in a dielectric or magnetic medium, we must recognize how the rotation angles vary with path length. In Figure 3, snapshots of the $\boldsymbol{\mathcal{E}}_{\pm}$ vectors at time t = 0 are sketched at regular intervals over a half cycle. As the waves progress from zero along the z-axis, the rotation angles $\varphi_{\pm}$ of the two vectors increase according to $\mp\beta z$, consistent with the images of the counter-rotating spirals of Figure 2 that make up a linearly polarized wave advancing with velocity ω/β. This concept is used to explain Faraday rotation of linear polarization and the origin of nonreciprocal effects in microwave and optical systems.

Nonreciprocal Birefringence

The importance of the two circular-polarization components arise in magnetized media where the propagation constants are not equal. In this situation, the spiraling modes shown in Figure 2 propagate at different velocities, creating an effect called magnetic circular birefringence (MCB). Birefringence is the property of a medium with two distinct propagation constants [1, 2] that result from the arrangement of internal dipole moments in a dielectric or magnetic medium.*

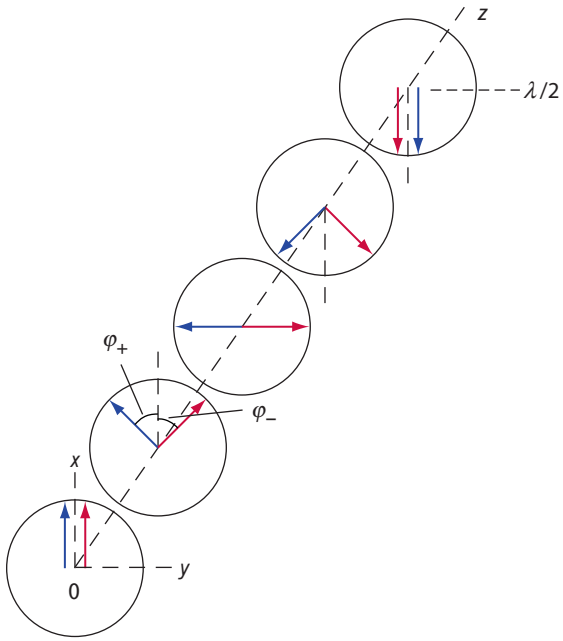

FIGURE 3. Snapshots at t = 0 of $\mathcal{E}_{\pm}$ in the x-y plane at successive $\lambda/8$ stages in a dielectric medium of propagation constant β. The rotation angles φ_{+} and φ_{-} of the respective RHCP and LHCP vectors are equal in magnitude because $\beta_{+} = \beta_{-} = \beta$. In situations where β_{+} and β_{-} differ, nonreciprocal action will occur that can be utilized for isolation or modulation purposes.

In a magnetic medium, MCB is caused by a difference in the product of the permittivity and permeability, i.e., $\varepsilon_{\pm}\mu_{\pm}$, between the two circular components. In the permeability case the magnetic dipoles from the combined quantum orbital and spin angular momenta of the individual ions produce the interaction with the propagating signal. It is important to remember the dual nature of orbital angular momentum, whereby an orbiting electron creates both a magnetic- and an

* In the pure dielectric case, magnetic moments have no influence on propagation. The material is usually a single crystal with a defined axis of symmetry, e.g., calcite or quartz, that presents a different permittivity, depending on whether the electric field of the linearly polarized TEM wave is parallel or perpendicular to the symmetry axis. In this case, the effects on signal polarization are reciprocal, i.e., independent of entry or exit port.

electric-dipole moment. In the permittivity case, the electric-dipole aspect of the orbital momentum produces the interaction, but the essential alignment of the individual dipoles for a collective result is accomplished by magnetic alignment.

In the pure magnetic-dipole case, the optimum interaction between the magnetic field $\mathcal{H}$ of the propagating TEM wave and the magnetic medium occurs when $\mathcal{H}$ is transverse to the axis of the magnetization vector **M** in the material, i.e., when the propagation is along the **M** axis. To create a resultant **M**, the individual magnetic-dipole moments must be aligned in a static magnetic bias field **H**.

What is most significant, however, is that the effects are nonreciprocal; i.e., they are reversed when either the entry and exit ports of the medium are reversed or alternatively, the direction of **M** is reversed. This feature of MCB creates the nonreciprocal propagation action of microwave and optical isolators and circulators that are often essential for radar and communication systems.

A common application of the nonreciprocal characteristic of these magnetized media for RF and optical transmission is illustrated in Figure 4, where a linearly polarized wave propagating parallel to **M** undergoes a polarization rotation of 45°. Note that the polarization angle of the return signal increases to 90° instead of being restored to zero. This property allows for the creation of two-port isolators, and three- and four-port circulators that are described later in the section entitled "Microwave and Optical Beam Isolators." In a TEM wave, the rotation of the axis of polarization is called Faraday rotation, and the basic mechanisms that cause it are dipole transitions—magnetic for RF wavelengths and electric in the optical bands.

Frequency-dependent permeability and permittivity arising from respective magnetic- and electric-dipole interactions with a propagating electromagnetic signal are the basis for the nonreciprocal effects. Although the wavelength regimes of the two phenomena are the microwave bands for permeability and the near-IR/visible for permittivity, the electromagnetic phenomenology is almost identical in both cases. The physical origins, however, differ in ways that require separate explanations. We first review the standard classical theory.

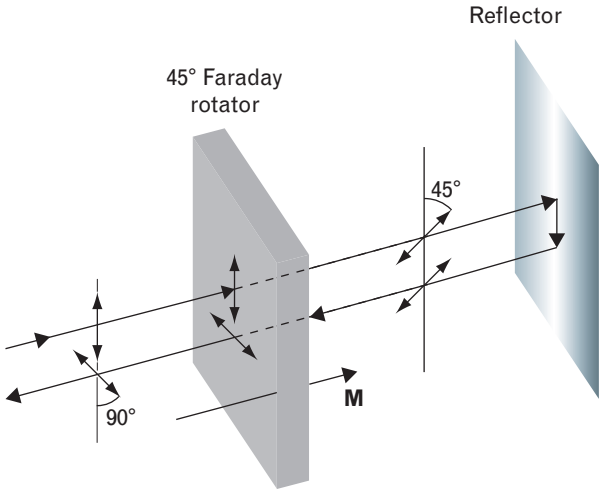

FIGURE 4. Basic demonstration of nonreciprocal action for signal isolation. The polarization of a reflected linear wave is rotated through 90° from the transmitted wave by two successive 45° rotations in passage through a magnetized Faraday-rotation medium. If the rotator had reciprocal propagation properties, the two 45° rotations would cancel and the polarization of the return signal would be unchanged.

Permeability and Permittivity Relations

For a medium with permeability tensor μ and permittivity tensor ε transmitting a TEM wave of angular frequency ω along the positive z axis—described earlier and illustrated with its counter-rotating circular modes in Figure 2 and 3—the relevant Maxwell relations [1, 2] at a fixed value of z can be written in electromagnetic units (emu) as

$$\nabla \times \nabla \times \mathcal{H} = \omega^2 [\varepsilon] \cdot [\mu] \cdot \mathcal{H}$$
$$\nabla \times \nabla \times \mathcal{E} = \omega^2 [\varepsilon] \cdot [\mu] \cdot \mathcal{E} .$$

The combined permeability/permittivity tensor can be expressed as

$$[\varepsilon] \cdot [\mu] = \begin{pmatrix} \varepsilon_0 & -i\varepsilon_1 & 0 \\ +i\varepsilon_1 & \varepsilon_0 & 0 \\ 0 & 0 & \varepsilon_z \end{pmatrix} \cdot \begin{pmatrix} \mu & -i\kappa & 0 \\ +i\kappa & \mu & 0 \\ 0 & 0 & \mu_z \end{pmatrix},$$

where the symbols ε_0, ε_1, μ, and κ are adopted to conform to accepted conventions. If all of the dipole moments are aligned with the z-axis, the eigenfunction solutions of the diagonalized matrix are the two orthogonal RHCP (+) and LHCP (–) modes of circular

polarization from Equations 4 and 5. The corresponding eigenvalues appear on the diagonal after the *x*-*y*-*z* coordinates are rotated about the *z*-axis, according to

$$[\varepsilon]\cdot[\mu]=\begin{pmatrix}\varepsilon_+\mu_+ & 0\\ 0 & \varepsilon_-\mu_-\end{pmatrix}, \tag{8}$$

where $\varepsilon_\pm\mu_\pm = (\varepsilon_0\mu + \varepsilon_1\kappa) \pm (\varepsilon_0\kappa + \varepsilon_1\mu)$ and $\varepsilon_z\mu_z$ is dropped because it is presumed that there is no active signal field component in the z direction. Note that $\varepsilon_z\mu_z$ reduces to $\varepsilon\mu$ when the off-diagonal elements are zero, which is consistent with no splitting of the circular modes. We show later in the section entitled "Resonance Dispersion Effects" that the permeability elements μ and κ are dependent on the density of magnetic moments, i.e., M. The permittivity elements ε_0 and ε_1 also depend on the density of electric dipoles. Since the RF and near-IR frequency regimes are far enough apart to be considered independent, the separate solutions $\mu_\pm = (\mu \pm \kappa)$ and $\varepsilon_\pm = (\varepsilon_0 \pm \varepsilon_1)$ become key analytical expressions for the present discussion. After rearrangement of Equation 8,

$$\mu = \frac{1}{2}(\mu_+ + \mu_-)$$

$$\kappa = \frac{1}{2}(\mu_+ - \mu_-)$$

and

$$\varepsilon_0 = \frac{1}{2}(\varepsilon_+ + \varepsilon_-)$$

$$\varepsilon_1 = \frac{1}{2}(\varepsilon_+ - \varepsilon_-)\,. \tag{9}$$

For both **M** and the propagation directed parallel to the *z*-axis in a semi-infinite medium, the propagation constant (with attenuation ignored) can be generalized for the (+) and (–) modes, and

$$\beta_\pm = \frac{\omega}{c}\sqrt{(\varepsilon_0\mu + \varepsilon_1\kappa) \pm (\varepsilon_0\kappa + \varepsilon_1\mu)}\,. \tag{10}$$

When β_+ and β_- are different, the clock-face images of Figure 3 serve to illustrate the origin of Faraday rotation of the polarization axis in the *x*-*y* plane, which occurs when the medium is magnetically biased, as shown in Figure 5.

In the RF case, $\varepsilon_1 = 0$, and the resultant $\mathcal{H}$ of the RHCP (+) and LHCP (–) vectors is rotated by [3]

$$\theta_F = \frac{\varphi_- + \varphi_+}{2} = \left(\frac{\beta_- - \beta_+}{2}\right)z$$

$$= \frac{\omega\sqrt{\varepsilon_0}}{2c}\left(\sqrt{\mu_-} - \sqrt{\mu_+}\right)z \approx -\frac{\omega}{2c}\sqrt{\frac{\varepsilon_0}{\mu}}\kappa z\,, \tag{11}$$

where $\kappa \ll \mu$ and θ_F is the Faraday-rotation angle for a distance z. Rotation of the optical $\mathcal{E}$ can be treated in the same manner by assuming $\mu = 1$ and $\kappa = 0$. From Equations 10 and 11 the off-resonance Faraday rotation can be as approximated by

$$\theta_F = \frac{\omega\sqrt{\mu}}{2c}\left(\sqrt{\varepsilon_-} - \sqrt{\varepsilon_+}\right)z$$

$$\approx -\frac{\omega}{2c}\sqrt{\frac{\mu}{\varepsilon_0}}\varepsilon_1 z\,,$$

where $\varepsilon_1 \ll \varepsilon_0$, the dielectric constant, which is assumed to be constant over the frequency range of interest [4].

Resonance Dispersion Effects

Because μ and ε resonate in different frequency regimes, the frequency dependence of μ can be analyzed with $\varepsilon = \varepsilon_0$ as the dielectric constant, and then the re-

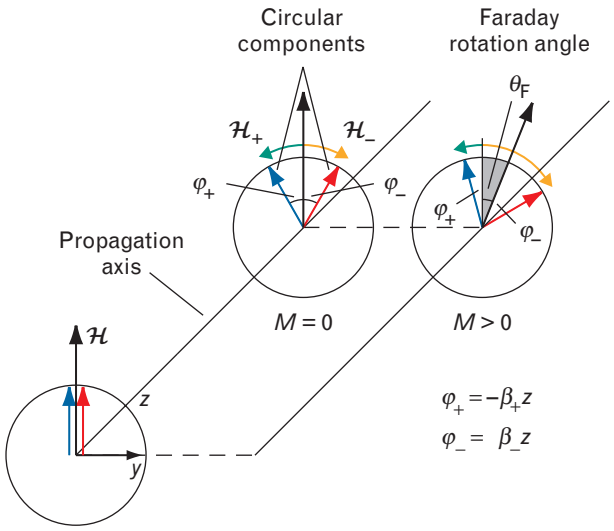

FIGURE 5. Schematic diagram of Faraday rotation in a ferrite magnetized along the *z*-axis of propagation. Phase angles φ_+ and φ_- of the corresponding $\mathcal{H}_+$ and $\mathcal{H}_-$ circular components are equal in magnitude and opposite in sign when the magnetization M is zero, thereby canceling the two field components along the *y*-axis. When M is not zero, $\varphi_+ < \varphi_-$, and the resultant $\mathcal{H}$ undergoes a net Faraday rotation θ_F.

sults applied by analogy to the ε case with $\mu = 1$. For low power conditions in the absence of damping effects, the respective resonance and nonresonance relations for the (+) and (–) circular permeabilities are derived from classical theory.

Magnetic-Dipole Resonance

From the general case of a fixed magnetization **M** (usually a collection of aligned spin moments each labeled by its quantum operator **S**) coupled to a static field **H** along the *z*-axis, the basic theory of magnetic resonance is derived from the equation of motion

$$\frac{d\mathbf{M}}{dt} = \gamma(\mathbf{M}\times\mathbf{H}),$$

where the vector $\mathbf{M}\times\mathbf{H}$ is normal to the plane containing **M** and **H**. Consequently, the resulting torque causes **M** to precess about **H**. The Larmor precession frequency is derived in most standard textbooks [5, 6], and is given by

$$\omega_0 = \gamma H ,$$

where the gyromagnetic constant γ = 2.8 GHz/kOe when ω is expressed in cycles/sec.

Magnetic resonance therefore occurs where an alternating (usually microwave or millimeter wave) magnetic $\boldsymbol{\mathcal{H}}$ field is applied perpendicular to **H**. Because a linearly polarized signal can be decomposed into two circularly polarized modes, the physical situation resembles that depicted in Figure 6(a). Only the circular component that rotates in the sense of the precessing moment is capable of continuously influencing the angle of **M** relative to the *z*-axis by creating a second torque $\mathbf{M}\times\boldsymbol{\mathcal{H}}$ normal to the $\mathbf{M}\times\mathbf{H}$ direction. By setting the frequency of the alternating field at $\omega = \omega_0$, $\boldsymbol{\mathcal{H}}$ will synchronize with the precession and apply a constant torque that will cause the cone half-angle to oscillate from full alignment with **H** to its opposite limit of π radians. The rotation of **M** away from **H** represents the dispersion and absorption of the signal.

In ferrimagnetic systems where **M** comprises multiple individual atomic moments, only small fractions of them complete this full rotation from the *z*-axis, and **M** departs only slightly from the *z*-axis under a low-amplitude $\boldsymbol{\mathcal{H}}$ signal. For these spontaneously magnetic systems, the permeabilities can be expressed in simplest terms as [7, 8]

$$\mu_\pm = 1 + \omega_M \rho_\pm , \tag{12}$$

where

$$\rho_\pm = \frac{\omega_0 \pm \omega}{\omega_0^2 - \omega^2 + \Gamma^2}$$

are the Lorentzian line shape functions for use as building blocks for combining polarization modes. The parameter $\omega_M = \gamma 4\pi M$ is the symbol used to represent the magnetization as an effective frequency. Note that only ρ_+ is resonant at $\omega = \omega_0$, but that ρ_- becomes comparable away from resonance. In Figure 7, the $\mu_\pm$ curves are sketched as a function of ω_0. Because it is presumed that signal loss would be minimized in any practical situation, the damping parameter, i.e., half-linewidth Γ, is assumed to be negligible under the conditions of interest. For the discussion that follows, the approximation $\rho_\pm = (\omega_0 \mp \omega)^{-1}$ is used.

Electric-Dipole Resonance

Nonreciprocal propagation can also occur in magnetic materials beyond the microwave and millimeter-wave bands where magnetic-dipole interactions prevail. In the optical bands, electric-dipole transitions driven by circularly polarized $\boldsymbol{\mathcal{E}}_\pm$ field components can produce magneto-optical Faraday rotation that is of major importance for fiber-optical and photonics technology. The physics that creates the birefringence involves transitions between atomic quantum states with orbital angular momentum split by spin-orbit coupling. The basic interactions are between rotating electric fields and a collection of electric dipoles with quantum states of frequency and polarization compatible with those of the stimulating radiation field. Since the individual dipole effects result from coupling of the momenta of orbiting electrons and magnetic spins within each dipole, the full combined effects of the electric dipoles can be achieved only by the collective alignment of each ionic spin, which usually requires a saturating magnetic field. The most general theoretical formalism must account for multiple contributing spectral pairs and their respective intensities. For the present purposes, we consider only one such spectral transition pair [9].

In the magnetic dipole case, the off-diagonal ele-

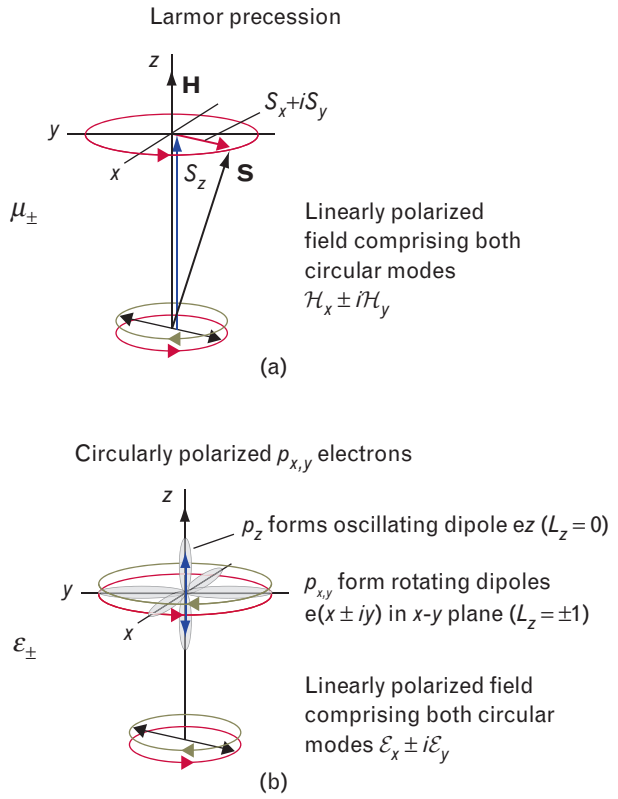

FIGURE 6. Rotating angular momentum diagrams: (a) spin angular momentum **S** precessing at the Larmor frequency about a *z*-axis magnetic field **H**, and driven by circularly polarized modes $\mathcal{H}_\pm$ in the *x*-*y* plane. Magnetic resonance occurs when signal frequency equals the Larmor precession frequency of the **S** vector; and (b) split $p_{x,y}$ orbital states of a magnetic molecule with orbital angular momentum L_z that rotates with the electric field $\mathcal{E}_\pm$ circular-polarization modes in the *x*-*y* plane. The *z*-axis orbital state p_z does not respond to the circular polarization. Optical transition frequencies correspond to the particular quantum state energies of the electric dipoles. Note that the amplitudes of $\mathcal{H}$ and $\mathcal{E}$ rotating with frequency ω in the *x*-*y* plane at $z = 0$ are expressed in complex scalar form to be consistent with the corresponding quantum wavefunctions of the transition states shown in Equation 7.

ment κ emerges directly from the solution of the classical Larmor model in the form of a spin-flip transition, as shown in Figure 6(a). A magnetic field creates a quantum energy splitting $\hbar\omega_0$ and determines which circular-polarization mode experiences resonance and which is unaffected, as defined by the $\mu_\pm$ relations of Equation 12 and illustrated in Figure 7. By contrast, there are two transition energies $\hbar\omega_0^a$ and $\hbar\omega_0^b$ in the birefringent electric-dipole case, one for each polarization mode. Therefore, a second set of permittivity solutions is required. For separate permittivities from this energy-level splitting, each counter-rotating orbital angular momentum state separated by $\hbar(\omega_0^a - \omega_0^b)$ must interact with the $\mathcal{E}_\pm$ of the appropriate circular mode.* The quantum wave functions for the electric dipoles that carry the opposing senses $L_z = \pm 1$ of orbital angular momentum correspond to the split energy levels of a ^{2}P orbital quantum term, as illustrated in Figure 6(b).

Since the line shape factors are identical for both magnetic and dielectric resonances, the magnetic resonance results can be adopted directly for each electric-dipole transition stimulated by circular polarization without loss of generality. The tensor elements ε_0 and ε_1 can be readily obtained by a reverse process. For dual transitions arising from split ^{2}P levels, individual mode permittivities $\varepsilon_\pm$ corresponding to states labeled a and b are determined first from an extension of Equation 12:†

$$\begin{aligned}\varepsilon_\pm &= 1 + \omega_E^a \rho_\pm^a + \omega_E^b \rho_\mp^b \\ &= 1 + \omega_E^a \left(\frac{1}{\omega_0^a \mp \omega} \right) + \omega_E^b \left(\frac{1}{\omega_0^b \pm \omega} \right).\end{aligned} \tag{13}$$

The quantum theory origin of ω_E is compared with its magnetic counterpart ω_M in the Appendix.

Tensor Element Functions

The real-part solutions for the tensor elements of permeability and permittivity for various cases can now be constructed with the aid of Equations 9, 12, and 13. The magnetic-dipole single transition solution is

$$\begin{aligned}\mu &= 1 + \frac{1}{2}\omega_M \left[\rho_+ + \rho_- \right] = 1 + \frac{\omega_M \omega_0}{\omega_0^2 - \omega^2} \\ \kappa &= \frac{1}{2}\omega_M \left[\rho_+ - \rho_- \right] = \frac{\omega_M \omega}{\omega_0^2 - \omega^2}.\end{aligned} \tag{14}$$

* In magneto-optical materials in which electric rather than magnetic dipoles provide the agents for splitting the (+) and (–) modes, the magnetic spin components of the dipoles must still be aligned in a magnetic field to produce the necessary alignment for a collective effect on a macroscopic scale.

† Planck's constant, $\hbar$, is absorbed into the ω terms for brevity.

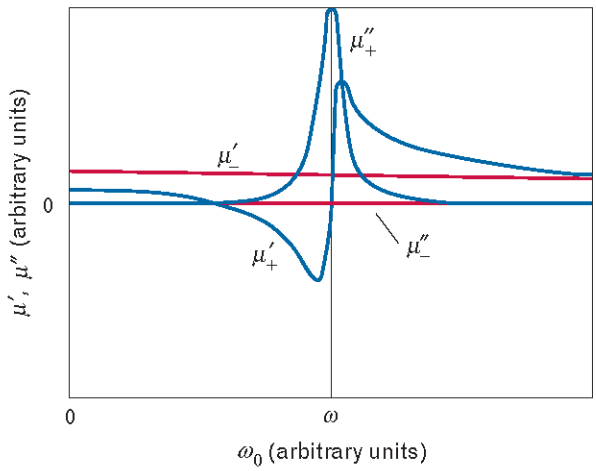

FIGURE 7. Graphical representation of Equation 12, where $\mu_\pm$ are plotted as a function of ω_0, revealing the dispersive nature of μ_+ and the insensitivity of μ_- to variations in frequency. To include line broadening with this generic calculation, we chose an appropriate value for the Lorentzian half-linewidth term that was added to the denominator, where it appears as Γ^2. In most applications where damping is to be minimized, the frequency range is either well below or well above ω_0, where $\mu''_\pm$ are zero. Note that the μ' and μ'' curves above are the real and imaginary parts of μ. This article is solely interested in the real part, and thus has named it μ throughout.

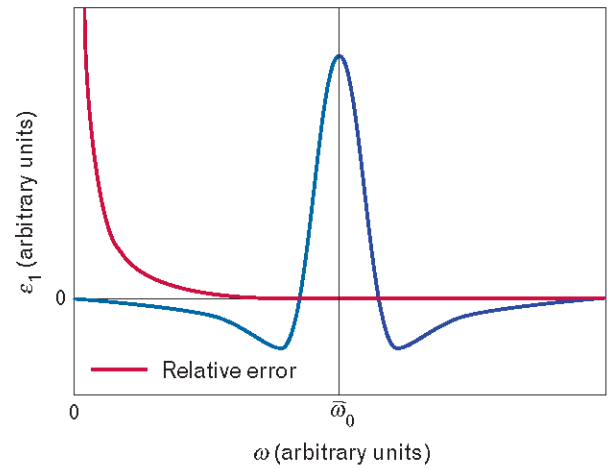

FIGURE 8. Model dispersion characteristic of the off-diagonal permittivity element ε_1 for the split excited state. The ε_1 curve is plotted as a function of ω with generic parameter values from the complete version of Equation 15. If the second (nonresonant) term is omitted (a standard approximation), the error introduced at low frequencies can be significant. The ratio of the erroneous permittivity to the correct one is plotted to actual scale and is seen to rise asymptotically as $\omega \to 0$. The resonance point $\bar{\omega}_0$ is the average of ω_0^a and ω_0^b.

The electric-dipole double transition solutions are

$$\varepsilon_0 = 1 + \omega_E \left[\frac{(\omega_0 - \omega)}{(\omega_0 - \omega)^2 - \Delta^2} + \frac{(\omega_0 + \omega)}{(\omega_0 + \omega)^2 - \Delta^2} \right]$$

$$\varepsilon_1 = -\omega_E \Delta \left[\frac{1}{(\omega_0 - \omega)^2 - \Delta^2} - \frac{1}{(\omega_0 + \omega)^2 - \Delta^2} \right], \qquad (15)$$

where $\omega_E^a = \omega_E^b = \omega_E$ and $2\Delta = \omega_0^a - \omega_0^b$.

In Equations 14 and 15 the half-linewidth parameter Γ is introduced by the straightforward substitution $\omega - i\Gamma \to \omega$, where it will appear in the denominators as Γ^2 [10]. In Figure 8, ε_1 is plotted as a function of ω to illustrate the type of curve characteristic of the transition $^2S \to {}^2P$ described in the appendix.

In the original derivation of Equation 15, the nonresonant term in ε_0 and ε_1 was ignored because it is negligible near resonance [11]. The use of this approximation has become standard practice, but as indicated, it can lead to significant errors at low frequencies [12], which is the regime of fiber-optic telecommunications.

Microwave and Optical Beam Isolators

The unidirectional propagation properties of circular polarization in magnetized media can be exploited in a number of device configurations where the RF vectors are orthogonal to the magnetization direction. Traditionally, waveguides have been used, as reviewed in B. Lax and K.J. Button [13]. In more recent years, microstrip and stripline geometries employing planar magnetic structures, often obtained by film deposition methods, have been under development. For the present instructional purpose, however, the simplest optical beam concept will be used.

A quasi-optical four-port microwave Faraday-rotation isolator/circulator was demonstrated at 35 GHz [14, 15]. As indicated schematically in Figure 9, the vertical axis of polarization is first rotated 45° clockwise as it passes through the magnetized ferrite disk that approximates a semi-infinite medium of appropriate thickness. After reflection, it undergoes an additional 45° rotation made possible by the nonreciprocal property of the magnetized ferrite and is then deflected by the wire-grid polarization filter, thereby accomplishing its isolator function of protecting the

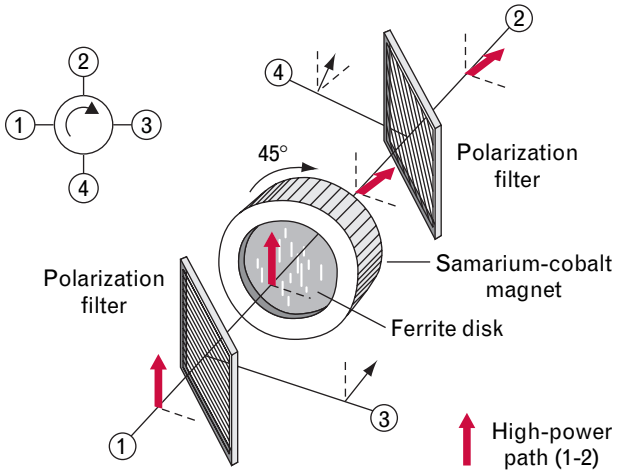

FIGURE 9. Diagram of the Lincoln Laboratory four-port quasi-optical Faraday-rotation circulator based on Figure 4. The device comprises a ferrite rotator disk magnetized in an external magnetic field supplied by a samarium-cobalt (SmCo) donut magnet, and two appropriately oriented linear polarization filters. The antireflection impedance-matching plates on either face of the ferrite are not shown.

signal source and the circulator function of directing the return signal into a receiver channel. For the design of the ferrite rotator element, Equations 11 and 14 are combined to give a total Faraday rotation:

$$\theta_F = -\frac{\omega\sqrt{\varepsilon_0}}{2c\sqrt{\mu}}\frac{\omega_M\omega}{\omega_0^2-\omega^2}d \approx \frac{\sqrt{\varepsilon_0}}{2c}\gamma 4\pi M\cdot d\ ,$$

where $\omega \gg \omega_0$ and $\mu \rightarrow 1$. As a consequence, the basic variables involved in the design of the ferrite element are M, the magnitude of the fixed magnetization **M**, and the element thickness d required for a 45° rotation angle.

A previous article by W.D. Fitzgerald described the insertion of this device in the Kiernan Reentry Measurements Site (KREMS) Ka-band Millimeter Wave Radar [16]. Figure 10(a) shows a cross section of the Faraday rotator unit with ferrite and dielectric anti-reflection disks stacked inside the donut-shaped samarium-cobalt (SmCo) permanent magnet that provides the field necessary to saturate the magnetic state of the ferrite. For this application, a temperature-insensitive ferrite derived from yttrium-iron garnet $Y_3Fe_5O_{12}$ (YIG) is used. Measured transmission characteristics are presented in Figure 10(b), where the isolation reaches 27 dB over a fractional bandwidth of 2 GHz. Applications of this principle have also been demonstrated at 16 and 95 GHz, where large amplitude signals produce high power densities in the quasi-optical beam.

In the near-IR telecommunication wavelength band centered at 1.55 μm, optical isolators for semiconductor laser sources are also commonly made as discrete components for insertion with fiber-optical circuits (networks). These devices involve 45° polarization rotation that is accomplished in the same manner as the microwave device, and have a rotator element that is also a magnetic garnet, but with electric-dipole transitions at the appropriate frequency. However, unlike the microwave rotator that operates with an energy splitting $\hbar\omega_0$ that can be adjusted directly by the applied magnetic field, the optical rotator cannot be

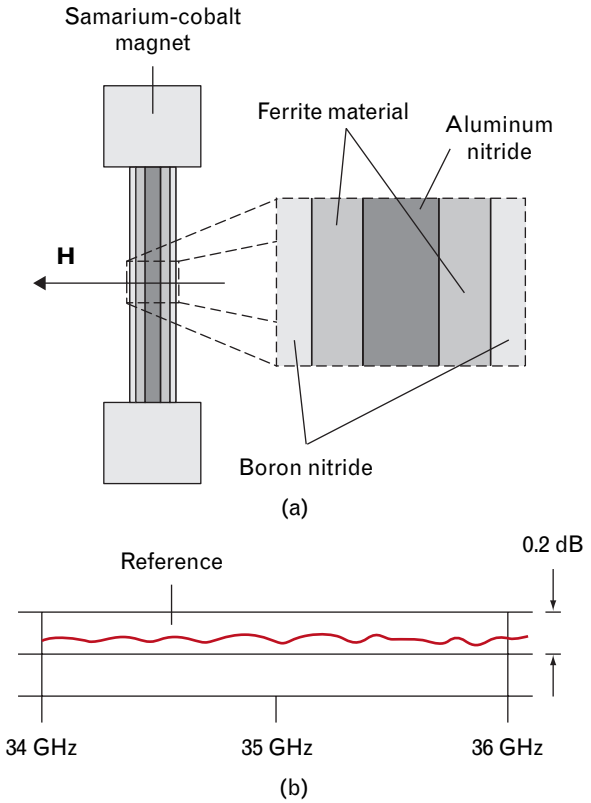

FIGURE 10. Details of the ferrite rotator element: (a) cross section of the dual-ferrite-disk design, which has a half-wavelength heat sink inserted between the ferrite halves: (b) measured insertion loss over the 34 to 36 GHz band. The only cooling is an air flow directed at the outer-face boron nitride quarter-wavelength impedance matching plates.

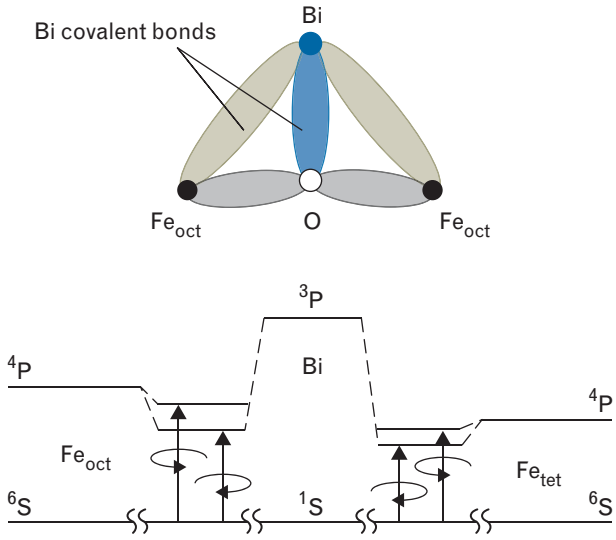

FIGURE 11. Molecular bonding source of the bismuth-enhanced electric-dipole transitions in the iron-garnet structure. The iron ions occupy oxygen sites of octahedral and tetrahedral coordination and interact with each other through the oxygen ions (magnetic superexchange). When bismuth is present, its excited ^{3}P orbital state couples to the excited ^{4}P states of the neighboring Fe$_{oct}$ and Fe$_{tet}$ ions to enhance the spin-orbit splitting and produce a larger ε_1. The energy-level model illustrates how these split transitions can produce the major magneto-optical lines of the $Y_{2.75}Bi_{0.25}Fe_5O_{12}$ (BiYIG) family.

tuned magnetically. Optimization of design is therefore dependent on the compatibility of quantum transition energies of matching semiconductor laser source and magnetic rotator. Furthermore, because of the microscopic dimensions dictated by the infrared wavelengths, purity of transmission cannot be obtained by polycrystalline (ceramic) media.

To magnify the splitting of the excited ^{2}P term, the conventional yttrium-iron-garnet composition were modified with the addition of bismuth Bi^{3+} ions in the Y^{3+} site, shown schematically as a molecule together with an abbreviated energy-level diagram in Figure 11. In a project sponsored by the Lincoln Laboratory Innovative Research Committee, the physical mechanism for the splitting by Bi^{3+} ions was explained in journal articles [17, 18], culminating in an MIT Department of Physics doctoral thesis [19]. The resulting theoretical models have become the standard for interpreting the magneto-optical properties of bismuth magnetic garnet isolators.

Each of the magnetically opposed iron sublattices of the garnet ferrite has its own set of spectral parameters. Calculated values of the off-diagonal permittivity ε_1 are obtained by subtraction of the computed contributions from the tetrahedral and octahedral oxygen-coordinated sites. An example of the accuracy of theory fit to measurement is given in Figure 12. For this exercise, Equation 15 (with the damping parameter Γ included) was used for the sublattice transitions at energies $\hbar\omega_0^{tet}$ = 2.6 eV, $\hbar\omega_0^{oct}$ = 3.15 eV, and a second $\hbar\omega_0^{tet}$ = 3.9 eV, respectively, for the compound $Y_{2.75}Bi_{0.25}Fe_5O_{12}$ (BiYIG). We must remark that the actual operating energy for the 1.55 μm wavelength is only 0.8 eV, which is far into the low-energy tails of the resonance lines and cannot be adjusted by external fields.

With single-crystal rotator disks, these devices have excellent performance, offering isolation ratios exceeding 40 dB and insertion losses below 0.5 dB over a range of wavelengths centered on the 1.55 μm telecommunications wavelength. Although YIG has a relatively low Faraday-rotation parameter (0.084°/μm

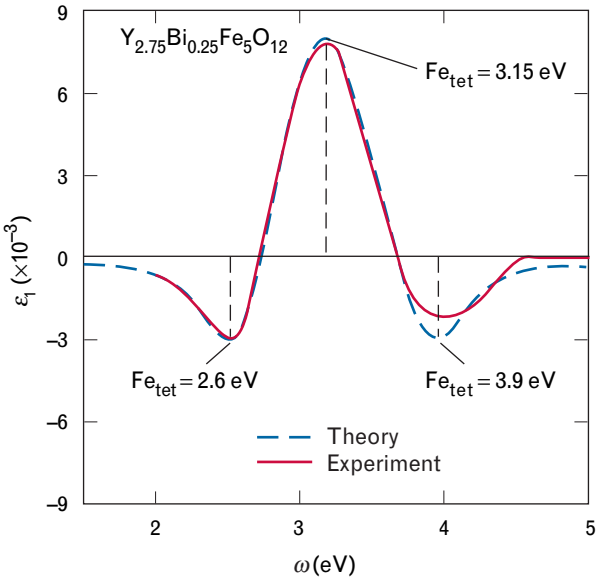

FIGURE 12. Comparison of theory to measurement data for the compound $Y_{2.75}Bi_{0.25}Fe_5O_{12}$. Energy splittings ω_0 are expressed in electron volts (eV) and indicate that the main magneto-optical transition at 3.15 eV originates from the octahedral Fe site. Two other transitions at 2.6 and 3.9 eV are attributed to Fe in the magnetically opposed tetrahedral sublattice. In fiber-optical transmission systems, the IR energy band is below 1 eV.

at 0.633 μm wavelength [20]), the substitution of bismuth into the yttrium sites increases the Faraday rotation dramatically, so that the fully substituted $Bi_3Fe_5O_{12}$ (BiIG) has a Faraday rotation of 7.8°/μm at 0.633 μm [21]. In practice, the garnet ferrite is a film deposited on a dielectric substrate by liquid-phase epitaxial (LPE) growth with the properties of a single crystal.

Present and Future Challenges

Because of their intrinsic nonreciprocal property, magnetic components remain as the only passive solution to isolation and circulation in RF or optical transmission systems. As a consequence, efforts are continuing to attain improvements in terms of greater power handling and efficiency, lower cost and, most significantly for photonic applications, integration with the ever-shrinking size of microelectronic circuitry.

High-Power Reflection Circulator

With the development of increasingly higher-power microwave- and millimeter-wave sources, the demands for greater efficiency of passive isolator and circulator components have also accelerated. Future requirements for advanced radar will challenge the power handling limits of the transmission concept described in the preceding section. Heat generated by absorption of the incident Gaussian-profiled signal beam localized at the center of the outer face of the ferrite element is the main issue. For pulsed-microwave operation, peak powers can in theory exceed 100 kW at millimeter wavelengths before nonlinear spin-wave thresholds are reached [22]. However, average heat dissipation of only a few kW will cause temperature increases that can degrade the ferrite-rotator performance by reducing the value of M. A more serious problem arises when thermal shock at the rotator surface can fracture the ceramic and lead to catastrophic failure.

In a second Lincoln Laboratory Innovative Research Program project [23–25], a novel modification of the quasi-optical concept was described, where the path length through the ferrite could be halved by designing a reflection configuration, as illustrated in Figure 13. This arrangement also permits simplification of the biasing magnet structure to allow for higher magnetization ferrite, and consequently thinner elements,

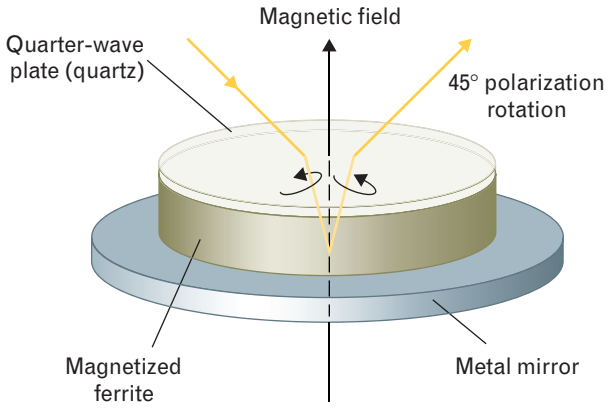

FIGURE 13. Generic concept of the 45° reflection Faraday rotator. Angle of incidence narrows by refraction inside the magnetized ferrite disk. Because the wave passes through the ferrite twice (each passage producing a 22.5° rotation) the thickness can be halved and only one quarter-wavelength impedance-matching plate is needed. The metal reflector plate can also serve as part of the external magnetic structure. The net result is a geometry that offers advantages of more efficient heat removal and a simpler magnetizing circuit capable of higher fields.

as well as a more efficient heat-removal configuration. A further advance could utilize a magnetically self-biased uniaxial type of ferrite (hexagonal structure) that can function at millimeter wavelengths without requiring an external magnetizing structure [26].

Integrated Photonics

The interest in integrated photonics has made it important to develop thin-film isolators that can be incorporated into a planar photonic circuit [27, 28]. Active magneto-optical devices such as modulators have also been proposed, based on the ability to change the Faraday-rotation angle by varying the magnetization **M** through a time-dependent magnetic bias field **H**(t) [29]. Magnetic garnet films have been grown by using chemical vapor deposition [30] and sputtering [31–33], but the most work has been in producing thin-film isolators by using LPE-grown garnet films on nonferrimagnetic garnet substrates [34–37]. The key element of these thin-film isolators is a ridge waveguide formed in the BiYIG film. A permanent magnet film may be overlaid to magnetize the waveguide, and a sequence of cladding layers and overlayers confine the light within the waveguide, control the birefrin-

gence of the structure, and tune the wavelength-dependent response. A basic structure is sketched in Figure 14. Dielectric birefringence, which originates both from the asymmetry of the rectangular shape of the waveguide and from effects such as growth-induced anisotropy and film internal stress, leads to elliptical polarization that must be minimized to obtain a high isolation ratio. Devices with up to 35 dB isolation ratios have been demonstrated [33–35, 37].

However, for integration with conventional microelectronics, the deposition of garnet-based magneto-optical materials onto non-garnet substrates such as silicon has presented problems because of crystallographic incompatibility. BiYIG compounds have lattice parameters much larger than that of common substrate materials. To overcome this difficulty, we have investigated other magnetic oxides. In any of these materials there is a trade-off between absorption and Faraday rotation, both of which depend on the spectral location of the electric-dipole transitions

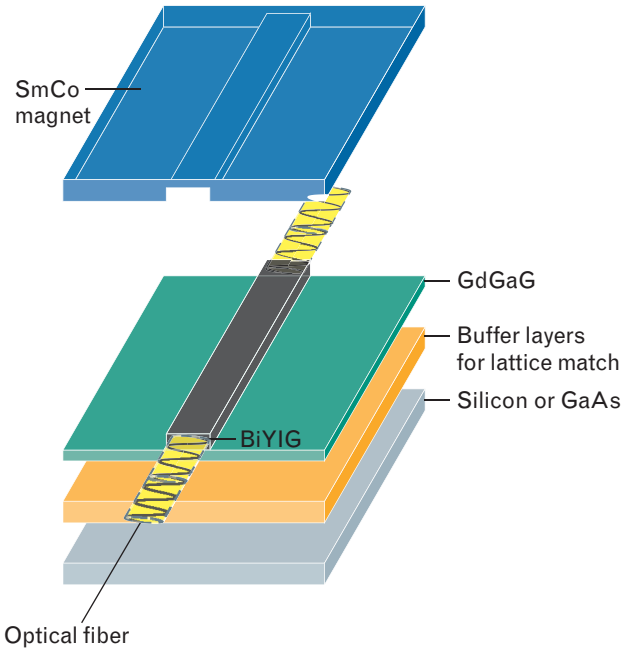

FIGURE 14. Generic concept of a magneto-optical planar structure with Faraday-rotation capability. An infrared signal is introduced from a fiber into a thick bismuth-yttrium-garnet-ferrite film, which is patterned in the shape of a waveguide grown epitaxially on a gadolinium-gallium garnet (GGG) substrate and clad to confine the propagating lightwave. The SmCo top layer is magnetized appropriately to generate a magnetic field along the axis of the BiYIG waveguide.

from magnetic ions. Maghemite (γFe_2O_3) and magnetite (Fe_3O_4), both with spinel crystal structures, can be grown relatively easily by vapor processes such as sputtering or laser ablation, and have high Faraday rotation, but their optical absorption is too high for them to make practical isolator materials [38]. Barium hexaferrite ($BaFe_{12}O_{19}$) films have also been studied [39]. Orthoferrites, with the generic formula ABO_3, have been extensively studied in the bulk form for their Faraday rotation [11], but there have been few studies of their properties as thin films [40], especially in the near-IR region. Another approach is to magnetically dope a material such as barium titanate, $BaTiO_3$, which has excellent optical transparency. Substitution of Fe for Ti leads to the development of dilute ferromagnetism that provides weak Faraday rotation [41]. As an example, $BaTi_{0.8}Fe_{0.2}O_3$ showed a rotation of only 0.02°/μm thickness at 1.55 μm, but its low absorption gives it a figure of merit (i.e., ratio of rotation to loss) that is much higher than that of materials such as maghemite [42]. Finally, magnetically doped semiconductors, although usually paramagnetic, may be promising as isolator materials for integrated photonic devices for certain wavelengths [43].

Acknowledgments

The authors are grateful for the contributions of Dr. Jerald A. Weiss to the invention of the quasi-optical millimeter-wave circulators. Engineering design information on the KREMS operational version was supplied by William D. Fitzgerald and David S. Rogers. Dr. Ashok Rajamani of MIT is acknowledged for his work on magneto-optical films for photonic-electronic circuit design, sponsored by the MIT Microphotonics Consortium. We also wish to recognize Dr. Hans P. Jenssen and Prof. Mildred S. Dresselhaus of MIT, and Vincent Vitto and the Innovative Research Program Committee at Lincoln Laboratory for their unyielding support and encouragement during the early stages of the magneto-optical part of this work.

REFERENCES

1. D.M. Pozar, *Microwave Engineering,* 2nd ed. (John Wiley, New York, 1998).
2. B. Lax and K.J. Button, *Microwave Ferrites and Ferrimagnetics* (McGraw-Hill, New York, 1962).
3. Lax and Button, *Microwave Ferrites and Ferrimagnetics*, p. 299.
4. J.F. Dillon, Jr., "Magneto-Optical Properties of Magnetic Garnets," *Physics of Magnetic Garnets: Proc. Int. School of Physics "Enrico Fermi" Course LXX, Varenna on Lake Como, Italy, 27 June–9 July 1977,* pp. 379–416.
5. A.H. Morrish, *The Physical Principles of Magnetism* (IEEE Press, New York, 2001), chap. 3.
6. G.E. Pake, *Paramagnetic Resonance* (W.A. Benjamin, New York, 1962), chap. 2.
7. Lax and Button, *Microwave Ferrites and Ferrimagnetics,* p. 156.
8. Pozar, *Microwave Engineering,* p. 504.
9. G.F. Dionne, "Simple Derivation of Four-Level Permittivity Relations for Magneto-Optical Applications," *J. Appl. Phys.* **97** (10), 2005, pp. 10F103-1–3.
10. N. Blömbergen, "Magnetic Resonance in Ferrites," *Proc. IRE* **44** (Oct.), 1956, pp. 1259–1269.
11. F.J. Kahn, P.S. Pershan, and J.P. Remeika, "Ultraviolet Magneto-Optical Properties of Single-Crystal Orthoferrites, Garnets and Other Ferric Oxide Compounds," *Phys Rev.* **186** (3), 1969, pp. 891–918.
12. G.A. Allen and G.F. Dionne, "Application of Permittivity Tensor for Accurate Interpretation of Magneto-Optical Spectra," *J. Appl. Phys.* **73** (10), 1993, pp. 6130–6132.
13. Lax and Button, *Microwave Ferrites and Ferrimagnetics,* chap. 12.
14. G.F. Dionne, J.A. Weiss, G.A. Allen, and W.D. Fitzgerald, "Quasi-Optical Ferrite Rotator for Millimeter Waves," *1988 IEEE MTT-S Int. Microwave Symp. Dig.* **1,** *New York, 25–27 May 1998,* pp. 127–130.
15. G.F. Dionne, J.A. Weiss, and G.A. Allen, "Nonreciprocal Magneto-Optics for Millimeter Waves," *IEEE Trans. Magn.* **24** (6), 1988, pp. 2817–2819.
16. W.D. Fitzgerald, "A 35-GHz Beam Waveguide System for the Millimeter-Wave Radar," *Linc. Lab. J.* **5** (2), 1992, pp. 245–272.
17. G.F. Dionne and G.A. Allen, "Spectral Origins of Giant Faraday Rotation and Ellipticity in Bi-Substituted Magnetic Garnets," *J. Appl. Phys.* **73** (10), 1993, pp. 6127–6129.
18. G.F. Dionne and G.A. Allen, "Molecular-Orbital Analysis of Magneto-Optical Bi-O-Fe Hybrid Excited States," *J. Appl. Phys.* **75** (10), 1994, pp. 6372–6377.
19. G.A. Allen, "The Magneto-Optic Spectra of Bismuth-Substituted Iron Garnets," Ph.D. Thesis, Dept. of Physics, MIT, Cambridge, Mass., 1994.
20. P. Hansen and J.-P. Krumme, "Magnetic and Magneto-Optical Properties of Garnet Films," *Thin Solid Films* **114** (1/2), 1984, pp. 69–107.
21. N. Adachi, V.P. Denysenkov, S.I. Khartsev, A.M. Grishin, and T. Okuda, "Epitaxial $Bi_3Fe_5O_{12}$ (001) Films Grown by Pulsed Laser Deposition and Reactive Ion Beam Sputtering Techniques," *J. Appl. Phys.* **88** (5), 2000, pp. 2734–2739.
22. E. Schlömann, J.J. Green, and U. Milano, "Recent Developments in Ferromagnetic Resonance at High Powers," *J. Appl. Phys*. **31** (supp. 5), 1960, pp. S386–S395.
23. B. Lax, J.A. Weiss, N.W. Harris, and G.F. Dionne, "Quasi-Optical Reflection Circulator," *IEEE Trans. Microw. Theory Tech.* **41** (12), 1994, pp. 2190–2197.
24. J.A. Weiss, N.W. Harris, B. Lax, and G.F. Dionne, "Quasi-Optical Ferrite Reflection Circulator Progress in Theory and Millimeter-Wave Experiments," *SPIE* **2250,** 1994, pp. 365–366.
25. N.W. Harris, G.F. Dionne, J.A. Weiss, and B. Lax, "Characteristics of the Quasi-Optical Reflection Circulator," *IEEE Trans. Magn.* **30** (6, pt.1), 1994, pp. 4521–4523.
26. M.R. Webb, "A mm-Wave Four-Port Quasi-Optical Circulator," *Int. J. Infrared Millimeter Waves* **12** (1), 1991, pp 45–63.
27. M. Levy, "The On-Chip Integration of Magnetooptic Waveguide Isolators," *IEEE J. Sel. Top. Quantum Electron.* **8** (6), 2002, pp. 1300–1306.
28. D.C. Hutchings, "Prospects for the Implementation of Magneto-Optic Elements in Optoelectronic Integrated Circuits: A Personal Perspective," *J. Phys. D* **36** (18), 2003, pp. 2222–2229.
29. W.E. Ross, D. Psaltis, and R.H. Anderson, "Two-Dimensional Magneto-Optical Spatial Light Modulator for Signal Processing," *Opt. Eng.* **22** (4), 1998, pp. 485–490.
30. B. Stadler, K. Vaccaro, P. Yip, J. Lorenzo, Y.-Q. Li, and M. Cherif, "Integration of Magneto-Optical Garnet Films by Metal–Organic Chemical Vapor Deposition," *IEEE Trans. Magn.* **38** (3), 2002, pp. 1564–1567.

31. M. Gomi, S. Satoh, and M. Abe, "Giant Faraday Rotation of Ce-Substituted YIG Films Epitaxially Grown by RF Sputtering," *Jpn J. Appl. Phys.* **27** (8), 1988, L1536.
32. B.J.H. Stadler and A. Gopinath, "Magneto-Optical Garnet Films Made by Reactive Sputtering," *IEEE Trans. Magn.* **36** (6), 2000, pp. 3957–3967.
33. T. Shintaku, "Integrated Optical Isolator Based on Nonreciprocal Higher-Order Mode Conversion," *Appl. Phys. Lett.* **73** (14), 1998, pp. 1946–1948.
34. M. Levy, R.M. Osgood, H. Hegde, F.J. Cadieu, R. Wolfe, and V. Fratello, "Integrated Optical Isolators with Sputter-Deposited Thin-Film Magnets," *IEEE Photonics Technol. Lett.* **8** (7), 1996, pp. 903–905.
35. R. Wolfe, J.F. Dillon, Jr., R.A. Lieberman, and V.J. Fratello, "Broad-Band Magneto-Optic Waveguide Isolator," *Appl. Phys. Lett.* **57** (10), 1990, pp. 960–962.
36. N. Sugimoto, H. Terui, A. Tate, Y. Katoh, Y. Yamada, A. Sugita, A. Shibukawa, and Y. Inoue, "A Hybrid Integrated Waveguide Isolator on a Silica-Based Planar Waveguide Circuit," *J. Lightwave Technol.* **14** (11), 1996, pp. 2537–2546.
37. R. Wolfe, R.A. Lieberman, V.J. Fratello, R.E. Scotti, and N. Kopylov, "Etch-Tuned Ridged Waveguide Magneto-Optic Isolator," *Appl. Phys. Lett.* **56** (5),1990, pp. 426–428.
38. T. Tepper, C.A. Ross, and G.F. Dionne, "Microstructure and Optical Properties of Pulsed-Laser-Deposited Iron Oxide Films," *IEEE Trans. Magn.* **40** (3), 2004, 1685–1690.
39. Z. Šimša, R. Gerber, T. Reid, R. Tesař, R. Atkinson and P. Papakonstantinou, "Optical Absorption and Faraday Rotation of Barium Hexaferrite Films Prepared by Laser Ablation Deposition," *J. Phys. Chem. Solids* **59** (1), 1998, pp. 111–119.
40. D.S. Schmool, N. Keller, M. Guyot, R. Krishnan, and M. Tessier, "Magnetic and Magneto-Optic Properties of Orthoferrite Thin Films Grown by Pulsed-Laser Deposition," *J. Appl. Phys.* **86** (10), 1999, pp. 5712–5717.
41. R. Maier and J.L. Cohn, "Ferroelectric and Ferromagnetic Iron-Doped Thin-Film $BaTiO_3$: Influence of Iron on Physical Properties," *J. Appl. Phys.* **92** (9), 2002, pp. 5429–5436.
42. A. Rajamani, G.F. Dionne, D. Bono, and C.A. Ross, "Faraday Rotation, Ferromagnetism, and Optical Properties in Fe-Doped BaTiO3," *J. Appl. Phys.* **98,** 063907, 2005.
43. H. Shimizu and M. Tanaka, "Magneto-Optical Properties of Semiconductor-Based Superlattices Having GaAs with MnAs Nanoclusters," *J. Appl. Phys.* **89** (11, pt 2), 2001, pp. 7281–7286.

APPENDIX: QUANTUM ORIGINS OF ω_M AND ω_E

Transition probabilities for magnetic and electric-dipole interactions with plane-wave radiation are explained by quantum mechanical time-dependent perturbation theory. Figure A shows semi-classical models for the resonance mechanisms. The parameter ω_M for a Zeeman-split $S = 1/2$ case is expressed as

$$\omega_M = \gamma 4\pi M = \left[\frac{g_e m_B}{\hbar}\right] 4\pi N g_e m_B S$$
$$= \frac{4\pi N}{\hbar}\left|\langle g|g_e m_B S_+|e\rangle\right|^2 \qquad (1)$$
$$\omega_M = \frac{4\pi N}{\hbar}\left|\left\langle +\frac{1}{2}\left|g_e m_B\left(S_x \pm iS_y\right)\right|-\frac{1}{2}\right\rangle\right|^2,$$

where $g_e m_B S_+$ is the magnetic-dipole moment of the right-hand circular polarized signal mode, m_B is the moment of the electron spin (the Bohr magneton), and the spectroscopic splitting factor $g_e = 2$ for an electron spin.*

For the pair of electric-dipole transitions between the ground state and the a and b split excited state shown in Figure B, the dipole energy of the orbital angular momentum operator for the right-hand and left-hand circular-polarization modes is expressed as $erL_\pm$. A parameter $\omega_E^{a,b}$ is defined analogously to Equation 1 above, according to

$$\omega_E^{a,b} = \frac{4\pi N}{\hbar}\left|\langle g|erL_\pm|e^{a,b}\rangle\right|^2$$
$$= \frac{4\pi N}{\hbar}\left|\left\langle \frac{z}{r}\left|er\left(L_x \pm iL_y\right)\right|\frac{x+iy}{r}\right\rangle\right|^2. \qquad (2)$$

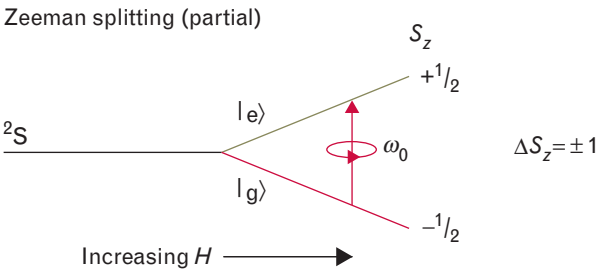

FIGURE A. Energy level diagrams corresponding to the physical mechanism diagrams of Figure 6 in the main text. The splitting shown corresponds to the wave functions in Equation 1 for partial Zeeman splitting dipole energy states.

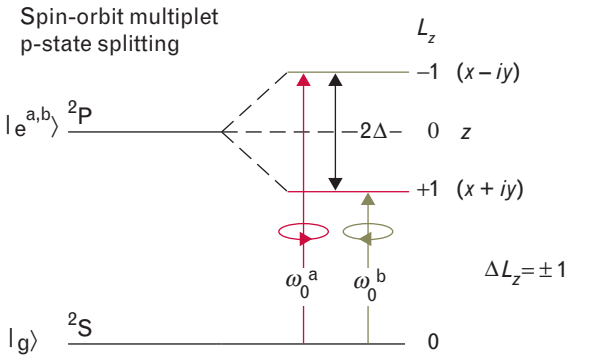

FIGURE B. Spin-orbit p-state splitting diagram corresponding to Equation 2. Splitting of these states is independent of H. The use of ω to represent energy assumes that the Planck's constant multiplier $\hbar$ is implicit. Only the split excited state (diamagnetic) case is shown.

* The use of ω to represent energy assumes that the Planck's constant multiplier $\hbar$ is implicit. Only the split excited state (diamagnetic) case is shown.

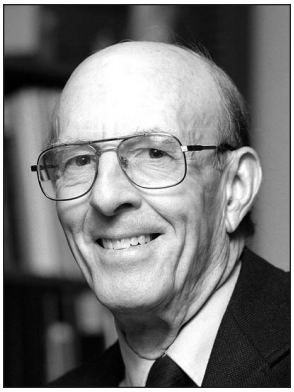

GERALD F. DIONNE
is a consultant for the Analog Device Technology group. He received a B.Sc. degree from the University of Montreal (Loyola College), a B.Eng. from McGill University, an M.S. degree from Carnegie-Mellon University, and a Ph.D. degree from McGill University with a thesis on electron paramagnetic resonance and relaxation. Before joining MIT, he was a member of the Department of Physics faculty at McGill, worked on semiconductor device development at IBM and the Sylvania Division of GTE, and investigated electron emission and cesium vapor ionization for thermionic energy conversion at Pratt & Whitney Aircraft. Since 1966 he has carried out research at Lincoln Laboratory in the fields of fundamental magnetism in solids, ferrimagnetic materials for microwave, millimeter-wave, and magneto-optical applications, millimeter- and submillimeter-wave radiometry, and electron emission. He pioneered in the development of ferrite devices that utilize the low resistance properties of superconductors for use in microwave phase shifters and high-Q tunable filters. He served as materials advisor to the DARPA-sponsored Ferrite Development Consortium in the 1990s. He is a fellow of the IEEE, the American Physical Society, and a member of the Materials Research Society and the Society of Sigma Xi.

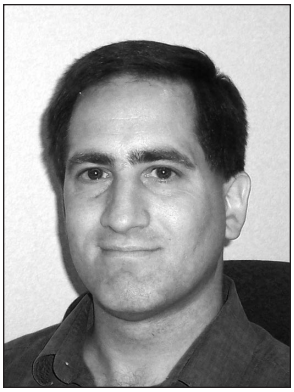

GARY A. ALLEN
is a staff engineer in the Components Research group at Intel Corporation in Hillsboro, Oregon. He has worked in the field of microlithography since joining Intel in 1996, and he is currently engaged in identifying and developing advanced lithography techniques for semiconductor manufacturing. He joined Lincoln Laboratory as a cooperative education student in 1985 in the Radar Measurements division. He maintained a part-time position with the Laboratory until starting his thesis work in investigating the magneto-optic effects of iron garnet materials, which was sponsored by Lincoln Laboratory. He received a B.S. degree in physics from Worcester Polytechnic Institute, and a Ph.D. degree in physics from MIT.

PAMELA R. HADDAD
is an assistant group leader in the Advanced Sensor Techniques group within the Sensor Systems division. She received a B.S. degree from the University of Massachusetts, an M.S. degree from the University of Michigan, and a Ph.D. degree from the University of Massachusetts, all in electrical engineering. Her doctoral work focused on the electromagnetic analysis of microstrip antennas using numerical techniques. She joined Lincoln Laboratory in 1995 where she specialized in the design of antennas and arrays for air defense radar systems. In August 2000, she moved to the Ballistic Missile Defense (BMD) Technology division to lead a team of analysts in the evaluation of discrimination algorithms and architectures for future BMD systems. She joined the Advanced Sensor Techniques group in January 2004 to concentrate on radar technology and algorithm development for the surface surveillance mission area. She is a member of the Lincoln Laboratory Advanced Concepts Committee, and has served as a part-time instructor in the graduate school at Northeastern University.

CAROLINE A. ROSS
is the Merton C. Flemings Career Development Professor of Materials Science and Engineering at MIT. She received B.A. and Ph.D. degrees from Cambridge University, U.K. She was a post-doctoral fellow at Harvard University and an engineer at Komag before coming to MIT in 1997. Her research interests are directed towards magnetic properties of thin films and small structures, particularly for data storage applications. Her group studies fabrication using sputtering, pulsed laser deposition, evaporation and electrodeposition combined with nanolithography and self-assembly methods, and measuring and modeling the magnetic behavior of the resulting films and nanostructures. She is a fellow of the American Physical Society and the Institute of Physics.

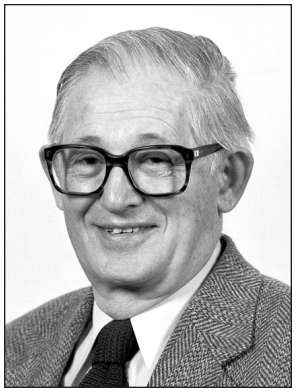

BENJAMIN LAX
is a consultant for the Optical Fabrication Facility in the Solid State Division working on laser and millimeter-wave radar. He is also Professor Emeritus and Director Emeritus at MIT. He received a B.M.E. degree in mechanical engineering from Cooper Union and a Ph.D. degree in physics from MIT. Prior to his arrival at Lincoln Laboratory, he taught electronics at Harvard, served as a radar officer at the MIT Radiation Laboratory and as radar consultant to Sylvania Electric Company. In 1951, he joined the Solid State group at Lincoln Laboratory where, in 1953, he became the head of the Ferrite group. In 1955 he was appointed the head of the Solid State group, which later became the Solid State division under his leadership. He was an associate director of Lincoln Laboratory, a professor of physics at MIT, and a member of the National Academy of Science. He founded the MIT Francis Bitter National Magnet Laboratory and served as its director until 1981. His scientific activities include microwave ferrites, plasma physics, magnetospectroscopy of solids, nonlinear optics, semiconductor and x-ray lasers, and quantum electronics. He has received numerous awards and citations, including the Buckley Prize of the American Physical Society, a Guggenheim Fellowship, and an award from the IEEE for his contribution to the development of the semiconductor laser.